Available online at www.sciencedirect.com
ScienceDirect
Ceramics International 37 (2011) 1219–1229
CERAMICS INTERNATIONAL
www.elsevier.com/locate/ceramint

Synthesis of silicon-substituted hydroxyapatite by a hydrothermal method with two different phosphorous sources

Alieh Aminian [a,*], Mehran Solati-Hashjin [a], Ali Samadikuchaksaraei [b], Farhad Bakhshi [a], Fazel Gorjipour [b], Arghavan Farzadi [a], Fattolah Moztarzadeh [c], Martin Schmücker [d]

[a] *Nanobiomaterials Lab, Biomaterials Group, Faculty of Biomedical Engineering, Amirkabir University of Technology, Tehran 15875-4413, Islamic Republic of Iran*
[b] *Department of Biotechnology, Cellular & Molecular Research Center, Iran University of Medical Science, Tehran 14155-6183, Islamic Republic of Iran*
[c] *Bioceramics Lab, Biomaterials Group, Faculty of Biomedical Engineering, Amirkabir University of Technology, Tehran 15875-4413, Islamic Republic of Iran*
[d] *German Aerospace Center (DLR), Institute of Materials Research, Köln, Germany*

Received 30 July 2010; received in revised form 28 September 2010; accepted 30 November 2010
Available online 21 January 2011

Abstract

Silicon-substituted hydroxyapatite (Si-HA) with up to 1.8 wt% Si content was prepared successfully by a hydrothermal method, using $Ca(NO_3)_2$, $(NH_4)_3PO_4$ or $(NH_4)_2HPO_4$ and $Si(OCH_2CH_3)_4$ (TEOS) as starting materials. Silicon has been incorporated in hydroxyapatite (HA) lattice by partially replacing phosphate (PO_4^{3-}) groups with silicate (SiO_4^{4-}) groups resulting in Si-HA described as $Ca_{10}(PO_4)_{6-x}(SiO_4)_x(OH)_{2-x}$. X-ray diffraction (XRD), Fourier transform IR spectroscopy (FTIR), inductively coupled plasma AES (ICP-AES) and scanning electron microscopy (SEM) techniques reveal that the substitution of phosphate groups by silicate groups causes some OH^- loss to maintain the charge balance and changes the lattice parameters of HA. The crystal shape of Si-HA has not altered compared to silicon-free reference hydroxyapatite but Si-incorporation reduces the size of Si-HA crystallites. Based on in vitro tests, soaking the specimens in simulated body fluid (SBF), and MTT assays by human osteoblast-like cells, Si-substituted hydroxyapatite is more bioactive than pure hydroxyapatite.

Keywords: Bioceramics; Hydrothermal synthesis; Silicon-substituted hydroxyapatite; Bioactivity

1. Introduction

Many different types of biomaterials have been used for bone replacement therapy [1,2] including calcium phosphate ceramics, which are well known for their successful biomedical applications. Among these ceramics, hydroxyapatite (HA), $Ca_{10}(PO_4)_6(OH)_2$, has been of considerable interest as a biomaterial for fabrication of implants and bone augmentations since its chemical composition is close to the bone mineral [2–4]. However, a disadvantage of using HA implants in comparison to bioactive glasses and glass–ceramics is that its reactivity with existing bone is low and the rate at which bone apposes and integrates with HA is relatively slow [5].

Recent studies have shown that bioactivity of synthetic hydroxyapatite can be enhanced by inclusion of intentionally added ionic substitutions, which create chemical compositions with more similarity to natural bone mineral [5,6]. Various ionic substitutions – both anionic and cationic – exist in the hydroxyapatite component of bone. For example carbonate ions are found at up to 8 wt%, as well as elements such as Na, Mg, K, Sr, Zn, Ba, Cu, Al, Fe, F, Cl and Si, which occur at trace levels ($\leq$1 wt%) [7–12]. Although the amount of these substitutions is small, they play important roles in the biological activity and interaction between the bone mineral and CaP-based implant materials by influencing the solubility, surface chemistry and charge, and morphology of the material [7–14].

Si in particular has been found to be essential for normal bone and cartilage growth and development. Synthetic CaP-based materials that include trace levels of Si in their structures

* Corresponding author at: Amirkabir University of Technology, Faculty of Biomedical Engineering, 424 Hafez Ave., Tehran 14155-6183, Islamic Republic of Iran. Tel.: +98 912 2887125; fax: +49 4212187404.
E-mail addresses: aminianalieh@gmail.com, a.aminian@aut.ac.ir (A. Aminian).

0272-8842/$36.00
doi:10.1016/j.ceramint.2010.11.044

demonstrate markedly increased biological performance in comparison to stoichiometric counterparts. This increase in biological performance can be attributed to Si-induced changes in the material properties and also to the direct effects of Si on physiological processes of the bone and connective tissue systems [4,5,7,15–18].

In this sense, addition of silicon to the apatite structure can improve the bioactivity of hydroxyapatite in the same way that it influences the bioactivity of bioactive glasses and glass–ceramics [4,15,19–24].

Silicon in fact was first identified as an important trace element in bone by Carlisle [25]. The substitution of silicate ions into hydroxyapatite lattice to produce single-phase bioceramics was reported by Gibson et al. [26]. Recent studies have shown that substitution of silicate for phosphate ions in hydroxyapatite enhances new bone formation *in vivo*; this effect was appeared to be enhanced by increasing the silicate substitution [4,5,27,28]. Silicate ion substitution has also been reported to enhance the formation of a poorly crystalline surface apatite layer on HA, when it is incubated in simulated body fluid (SBF) [5,23]. Already in the 1970s several groups demonstrated that bone mineralization requires a minimum concentration of soluble silicon [1–29]. Hench reported that deterioration in the proliferation and function of osteoblasts due to osteopenia and osteoporosis is related to the loss of biologically available silicon [30]. Scientists reported that bone cells proliferate more rapidly in the presence of soluble silicon [30].

These studies indicate the possible advantages of silicon incorporation into the structure of biomaterials intended for bone tissue regeneration applications. Therefore, to take advantage of the positive biological effects of silicon, Si-substituted hydroxyapatite (Si-HA) has been developed. Si-HA has been synthesized by several methods [1–8,13–31], each having its own advantages and disadvantages. Ruys [32] suggested the use of sol–gel procedure, however, these materials, besides the hydroxyapatite phase, include other crystalline phases depending on the substitution degree of silicon. Boyer et al. [33] conducted studies on the synthesis of Si-HA by solid state reaction, but in these cases the incorporation of secondary ion, like lanthanum or sulphate, was involved. Gibson et al. [34] and Kim et al. [25] synthesized silicon-containing hydroxyapatite by using a wet-chemical method, however, sintering at high temperature usually leads to bigger crystal size. Tian et al. [18] used mechanochemical method for synthesis of Si-HA, but in this method, conventional milling equipment and aqueous phase are essential. On the other hand, in this method heat temperature is not controllable.

Hydrothermal techniques usually result in materials with high degree of crystallinity and a Ca/P ratio close to the stoichiometric value. Crystal sizes obtained by hydrothermal syntheses are in the range of nanometers to micrometers [15,16,18,35,36]. The hydrothermal method has many benefits over the mentioned above, in fact, only hydrothermal methods and precipitation methods led to the formation of monophase materials [36].

The aim of this study is to synthesize approximately pure Si-substituted hydroxyapatite with controlled silicate amount by hydrothermal method and also to investigate the effect of different phosphorus sources on the amount of Si-incorporation in hydroxyapatite structure. Moreover, the influence of Si on the bioactivity of Si-HA is evaluated by soaking the samples in SBF (simulated body fluid) and monitoring the surfaces of them in different soaking times with SEM images and also with MTT assays using human osteoblast-like cells.

2. Materials and methods

2.1. Synthesis of HA and Si-HA

Stoichiometric hydroxyapatite and Si-substituted hydroxyapatite were synthesized by hydrothermal method using $Ca(NO_3)_2{\cdot}4H_2O$ (Prolabo Merck Eurolab No. 22384.298), $(NH_4)_3PO_4$ (Ridel – de Haen No. 05447) or $(NH_4)_2HPO_4$ (Merck No. 1.01207) and $Si(OCH_2CH_3)_4$: (TEOS) (Merck No. 8.00658) as sources of Ca, P and Si, respectively. Two series of powders were synthesized with two different phosphorus sources (for series 1: using $(NH_4)_3PO_4$ and for series 2: using $(NH_4)_2HPO_4$). The amount of reagents (Tables 1 and 2) was calculated on the assumption that silicon would substitute phosphorus.

The $Ca(NO_3)_2$ solution (0.5 M) was prepared keeping the pH higher than 10.0. Simultaneously the $(NH_4)_3PO_4$ solution (0.25 M) for series 1 or the $(NH_4)_2HPO_4$ solution (0.25 M) for series 2 was prepared and their pHs were kept higher than 11.0 by the addition of NH_3 solution (Merck No. 1.05426). $Ca(NO_3)_2{\cdot}4H_2O$ solution containing 0.2 g polyethylene glycol was added drop-wise to $(NH_4)_3PO_4$ and TEOS solutions or $(NH_4)_2HPO_4$ and TEOS solutions, respectively. The reaction mixtures were stirred for 0.5 h followed by hydrothermal treatment at 200 °C for 8 h. The resulting precipitates were washed three times, and then dried at 100 °C for 12 h. A fraction of each as-prepared samples was treated at 800 °C for 1 h in air.

Table 1
Quantities of reactants used and the measured wt% of Si of the samples using $(NH_4)_3PO_4$ as phosphorus source (series 1).

Samples	$n(Ca(NO_3)_2)$/mol	$n((NH_4)_3PO_4)$/mol	n(TEOS)/mol ($\times10^{-4}$)
HA T0.0SC[a]	0.025	0.0150	0.00
0.8 wt%Si-HA T0.8SC[a]	0.025	0.0143	0.71
1.5 wt%Si-HA T1.5SC[a]	0.025	0.0132	1.34
1.5 wt%Si-HA T1.5SR[b]	0.025	0.0132	1.34

[a] C: calcinated.
[b] R: not calcinated.

Table 2
Quantities of reactants used and the measured wt% of Si of the samples using $(NH_4)_2HPO_4$ as phosphorus source (series 2).

Samples	$n(Ca(NO_3)_2)$/mol	$n((NH_4)_2HPO_4)$/mol	n(TEOS)/mol ($\times 10^{-4}$)
HA D0.0SC[a]	0.025	0.0150	0.00
0.8 wt%Si-HA D0.8SC[a]	0.025	0.0143	0.71
1.5 wt%Si-HA D1.5SC[a]	0.025	0.0132	1.34
1.5 wt%Si-HA D1.5SR[b]	0.025	0.0132	1.34

[a] C: calcinated.
[b] R: not calcinated.

2.2. Samples preparation

0.3 g of each powder series was compacted (the applied pressure is less than 10 bar) to discs (0.5 cm in diameter and 1 mm in height) using a laboratory press. Powder compacts were used for MTT assays and incubation in simulated body fluid (SBF).

2.3. Preparation of SBF

To determine the changes on the surface of HA and Si-HA and to study superficial HA nucleation, powder compacts of both series were incubated in simulated body fluid (SBF), at 37 °C, for different periods of time between 1 and 14 days. The SBF solution was prepared by dissolving reagent-grade NaCl, KCl, $NaHCO_3$, $MgCl_2{\cdot}6H_2O$, $CaCl_2$ and KH_2PO_4 into distilled water and buffered at pH 7.25 with trishydroxymethyl aminomethane (TRIS) and HCl 1 N at 37 °C [37,38].

2.4. Characterization

The chemical composition (Ca, P, Si contents) was determined by inductively coupled plasma (ICP) atomic emission spectroscopy using an ICP – AES ARL – 3410 spectrometer. The phase compositions of powders were determined using X-ray diffraction (XRD). The XRD data were collected over 2θ range of 10–60° with a step size of 0.02° by a Siemens D500 diffractometer (40 kV and 30 mA) using Cu-Kα radiation (1.5418 Å). Phase identification was achieved by comparing the diffraction patterns of HA and Si-HA with ICDD (JCPDS) standards (card No. 09-0432). The average crystallite size of the samples was calculated by using the Scherrer formula. For further structural and compositional investigations Fourier transform infrared (FTIR) spectroscopy (Vector 33) was employed running in transmission mode using KBr pellets.

A Philips XL30 scanning electron microscopy (SEM) was used for microstructural characterization of HA and Si-HA samples before and after incubation for different periods of time in simulated body fluid. To avoid charging effects samples were sputter-coated with gold (Bal-Tec, Scdoos).

The cell-disc constructs were washed with PBS three times and fixed in a solution containing 2.5% (v/v) glutaraldehyde in 0.1 M PBS for 2 h. Then, the cell-scaffold constructs were soaked in 0.1% (v/v) osmium tetroxide (OsO_4) in 0.1 M PBS for 30 min, and washed again with PBS. The samples were dehydrated in graded acetone series (30, 50, 75, and 100%) and maintained in 100% acetone before freeze-drying (Boc-Edwards, Crawley, UK) for 6 h. The discs containing cells were sputter coated with gold (Bal-Tec, Scdoos), and viewed using the scanning electron microscopy (Philips, XL-30) at accelerating voltage of 20 keV.

2.4.1. Crystallite size and crystallinity

The average crystallite size of the samples can be calculated using the Scherrer formula, Eq. (1) [16,27]:

$$D_{hkl} = \frac{k\lambda}{\cos\theta\sqrt{\omega^2 - \omega_0^2}} \quad (1)$$

where $D_{(h\ k\ l)}$ is the crystallite size (nm); k is the shape coefficient, 0.9; λ is the wave length (nm); θ is the diffraction angle (°); ω corresponds to experimental full width at half maximum (FWHM) obtained for each sample; ω_0 corresponds to standard FWHM [16,27].

The degree of crystallinity, corresponding to the fraction of crystalline phase present in the examined volume can be estimated by X-ray diffraction data according to Eq. (2) [17,39]:

$$X_C \approx 1 - \left(\frac{V_{1\,1\,2/3\,0\,0}}{I_{3\,0\,0}}\right) \quad (2)$$

where X_C is the crystallinity degree, $I_{3\,0\,0}$ is the intensity of (3 0 0) reflection and $V_{1\,1\,2/3\,0\,0}$ is the intensity of the hollow between (1 1 2) and (3 0 0) reflection [17,39].

2.5. Cell culture

The human osteoblast-like cells, Saos-2 (National cells Bank of Iran), were cultured in Dulbecco's modified eagle's medium (DMEM) supplemented with 10% fetal bovine serum (FBS), 500 U/ml penicillin and 200 mg/L streptomycin (all from GIBCO Invitrogen, Germany). The cell suspension was transferred into 96 well culture plates and incubated at 37 °C, in a humidified atmosphere of 5%CO_2–95% air. Cultures were passaged and harvested by trypsinizing with 1 mM EDTA/0.25% trypsin digestion (0.05% [v/v] trypsin–0.53 mM EDTA in 0.1 M phosphate-buffered saline [PBS] without calcium or magnesium; GIBCO Invitrogen, Germany). Discs (made by different synthesized powders) were sterilized by exposing each side to UV light for 30 min. The sterilized discs were rinsed with PBS for three times before soaking in culture medium for 2 h. Equal numbers of osteoblast cells (50,000 cells for each sample) were then seeded on the surface of discs and

Table 3
Chemical analysis of the samples.

Samples	wt%			Weight ratio		Atomic ratio	
	Ca	P	Si	Ca/P	Ca/(P + Si)	Ca/P	Ca/(P + Si)
HA (T0.0SC)	39.88	18.49	0.00	2.157	2.157	1.667	1.667
0.8 wt% Si-HA (T0.8SC)	39.79	17.77	0.72	2.24	2.152	1.73	1.656
1.5 wt% Si-HA (T1.5SC)	39.75	17.19	1.35	2.312	2.144	1.787	1.657
HA (D0.0SC)	39.79	18.54	0.00	2.146	2.146	1.666	1.666
0.8 wt% Si-HA (D0.8SC)	39.73	17.9	0.65	2.22	2.142	1.715	1.649
1.5 wt% Si-HA (D1.5SC)	39.70	17.28	1.27	2.297	2.140	1.776	1.654

the culture medium was changed every other day. The proliferation rate was compared with the osteoblasts cultured on standard plastic surfaces by 3-(4,5-dimethylthiazol-2-yl)-2,5-diphenyltetrazolium bromide (MTT) assay. MTT test was performed according to the manufacturer's (Sigma, Germany) instructions and the optical density (OD) was recorded at a wavelength of 570 nm. A blank OD value was reduced from each sample's reading.

3. Results and discussion

3.1. Chemical composition

The chemical compositions of the Si-substituted samples as determined by ICP are shown in Table 3 together with the calculated Ca/P and Ca/(P + Si) ratios. The silicon content is lower than that of the corresponding amount of starting material in both series, which implies that some of the silicon ions remain in the mother liquor solution after precipitation. Because of the presence of CO_2 in solution during the synthesis, carbonate groups can replace some phosphorus sites and hence carbonated apatite was formed; as evidenced by FTIR technique. As a consequence of the incorporation of carbonate groups on PO_4 sites the amount of phosphorus substitution by silicon is reduced [8,26].

The present results show that $(NH_4)_3PO_4$ as phosphorus source is more effective than $(NH_4)_2HPO_4$ in terms of silicon incorporation into hydroxyapatite. Hence, preparing more almost pure Si-HA is possible when $(NH_4)_3PO_4$ is used as phosphorous source, in this case, the actual Si content is close to expected Si content.

3.2. Phase characterization

X-ray diffraction patterns of powders of series 1 and 2 are shown in Figs. 1 and 2, respectively. The X-ray diffraction patterns of samples calcined at 800 °C for 1 h indicate that the diffraction peaks of both series can be indexed based on JCPDS Card No. 09-0432 and do not reveal the presence of any phases related to a silicon oxide or other calcium phosphate species. In a first order approximation silicon substitution does not affect the diffraction pattern of hydroxyapatite.

Although the XRD patterns of both Si-HA series virtually correspond to that of pure HA, the diffraction peaks lose intensity with increasing Si content, proving a progressive loss of crystallinity.

Lattice parameters of pure and Si-substituted hydroxyapatite samples of both groups were determined by Rietveld structure refinement of X-ray diffraction data of each sample sintered at 800 °C for 1 h [15,16,40]. Unit cell parameters and unit cell volume of the samples are listed in Table 4.

Table 4 shows that silicon substitution results in a decrease in the *a*-axis and an increase in the *c*-axis of the unit cell of hydroxyapatite. These results were observed in both powder series. These findings are in good agreement with data recently published by Landi [8,39], Tang et al. [16], and Botelho [15,23,31].

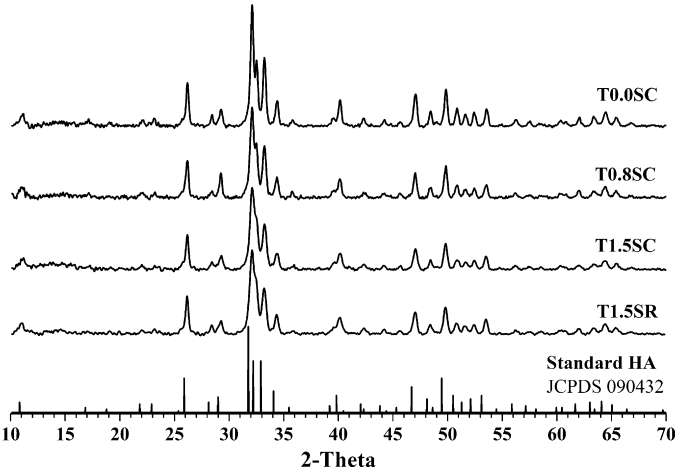

Fig. 1. XRD patterns of HA and Si-HA samples of series 1.

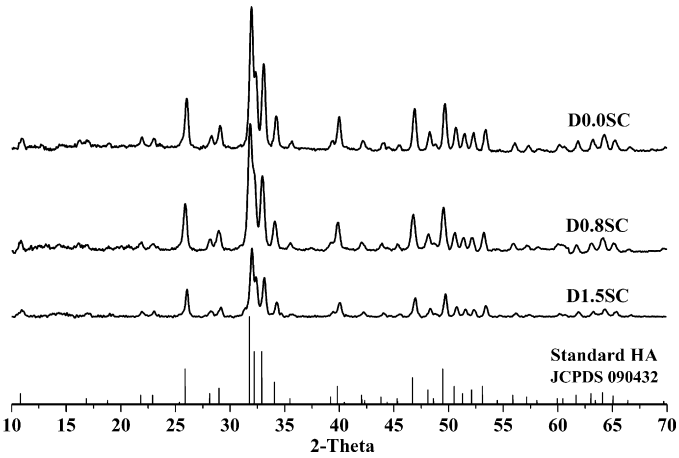

Fig. 2. XRD patterns of HA and Si-HA samples of series 2.

Table 4
Lattice parameters of HA and Si-HA.

Samples	a (Å)[a]	c (Å)[b]	v (Å^3)
HA (T0.0SC)	9.4082	6.8735	526.8921
0.8 wt% Si-HA (T0.8SC)	9.4065	6.8740	526.74
1.5 wt% Si-HA (T1.5SC)	9.4056	6.8790	527.0223
1.5 wt% Si-HA (T1.5SR)	9.4060	6.8794	527.113
HA (D0.0SC)	9.4185	6.8740	528.0848
0.8 wt% Si-HA (D0.8SC)	9.4160	6.8746	527.8505
1.5 wt% Si-HA (D1.5SC)	9.4158	6.8774	528.0319

[a] Uncertainty: ±0.00005.

Crystallite sizes calculated via the Scherrer formula are listed in Table 5. By application of the Scherrer formula crystal sizes of c. 50 nm were estimated for pure HA and for samples containing 0.8 wt% SiO_2. The crystal size of HA samples containing 1.5% SiO_2, however, is significantly smaller (c. 35 nm) irrespective the phosphorous source. The crystallinity degrees of different samples are listed in Table 6.

Table 6 shows that silicon incorporation increases structural disorder (or decreases crystallinity, respectively). Since Si-substitution in series 1 is higher than in series 2, samples of the former series show a more pronounced decrease in crystallinity.

FTIR was used to study the as-prepared and heat-treated powders to quantify the effect of the silicon substitution on the different functional groups, such as hydroxyl and phosphate groups of hydroxyapatite. All FTIR spectra (Figs. 3 and 4) illustrate the characteristic of OH^- band at 3570 cm^{-1} and PO_4^{3-} bands between 960 and 1100 cm^{-1} (1100, 1090, 1030 and 960 cm^{-1}) and 450 and 660 cm^{-1} (630, 600, 570 and 470 cm^{-1}) associated with HA. Broad bands of adsorbed water (3000–2850 cm^{-1}) were also present, as were weak bands in the region associated with the CO_3^{2-} vibration mode (1550–1410 cm^{-1}). The present absorption spectra, which are in close agreement with previous studies [15,16,19,20,23,26,39] indicate that CO_3^{2-} groups have substituted both PO_4^{3-} and OH^- groups in the HA structure.

Additional three low intensity bands appear at approximately 490, 760 and 890 cm^{-1}, which do not appear in reference HA samples. These three peaks have been attributed to the presence of SiO_4^{4-} groups in the apatite structure [15,16,25,39–42] and hence are regarded as specific features of Si-HA. Incorporation of silicon into hydroxyapatite

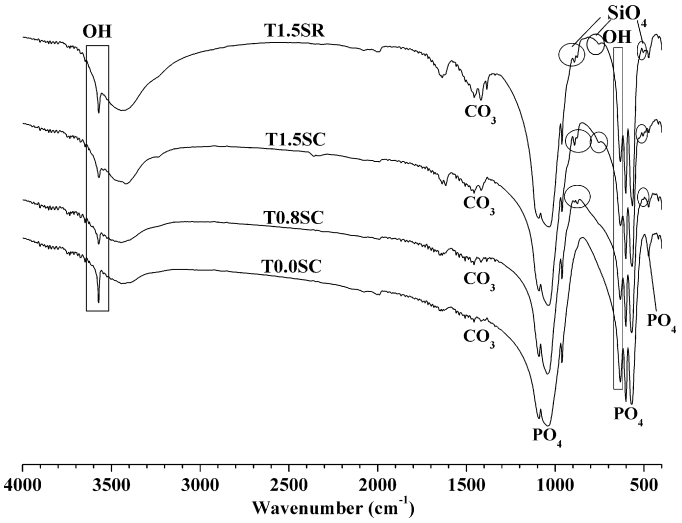

Fig. 3. FTIR patterns of HA and Si-HA samples of series 1.

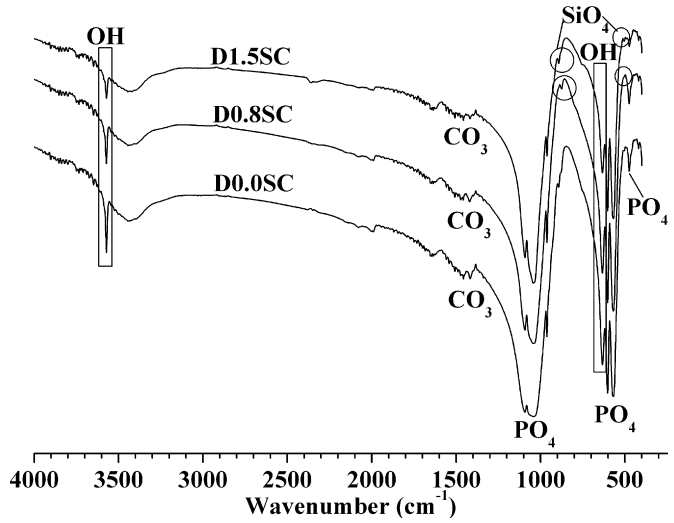

Fig. 4. FTIR patterns of HA and Si-HA samples of series 2.

($Ca_{10}(PO_4)_{6-x}(SiO_4)_x(OH)_{2-x}$) also changes hydroxyl stretching bands at 630 and 3570 cm^{-1}. The substitution of PO_4^{3-} by SiO_4^{4-} reduces the amount of hydroxyl groups required for charge balance. Moreover, as the Si content is increased, there is a strong intensity loss of the CO_3^{2-} related absorption bands

Table 5
Calculated average crystallite size of HA and Si-HA via the Scherrer formula.

Samples	T0.0SC	T0.8SC	T1.5SC	T1.5SR	D0.0SC	D0.8SC	D1.5SC
Average crystallite size (nm)	51	51	35	35	52	51	36

Uncertainty: ±5 nm.

Table 6
Estimated crystallinity degree of samples.

Samples	T0.0SC	T0.8SC	T1.5SC	T1.5SR	D0.0SC	D0.8SC	D1.5SC
Crystallinity degree (%)	80.75	79.05	68.80	50.26	85.29	76.66	74.42

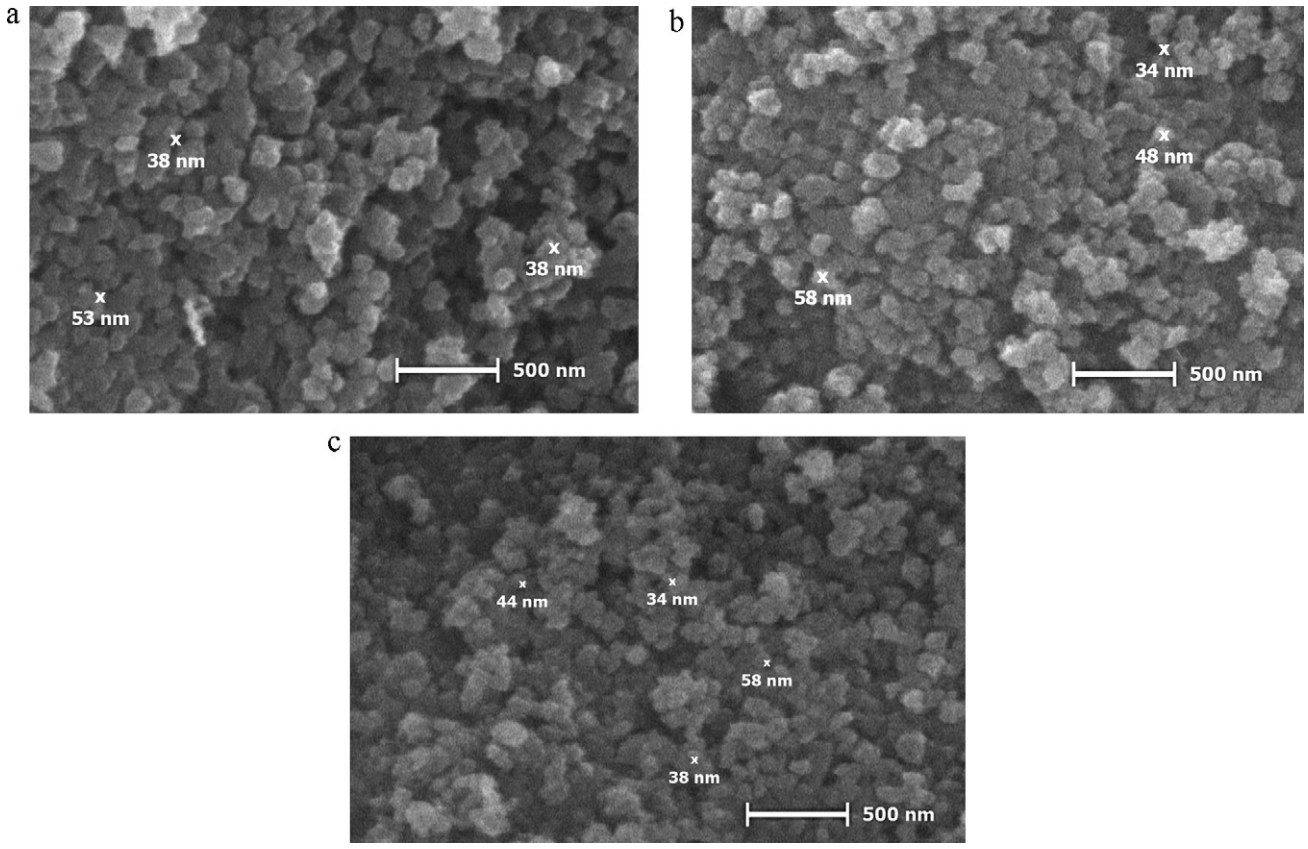

Fig. 5. SEM images of T0.0SC (a), T0.8SC (b) and T1.5SC (c).

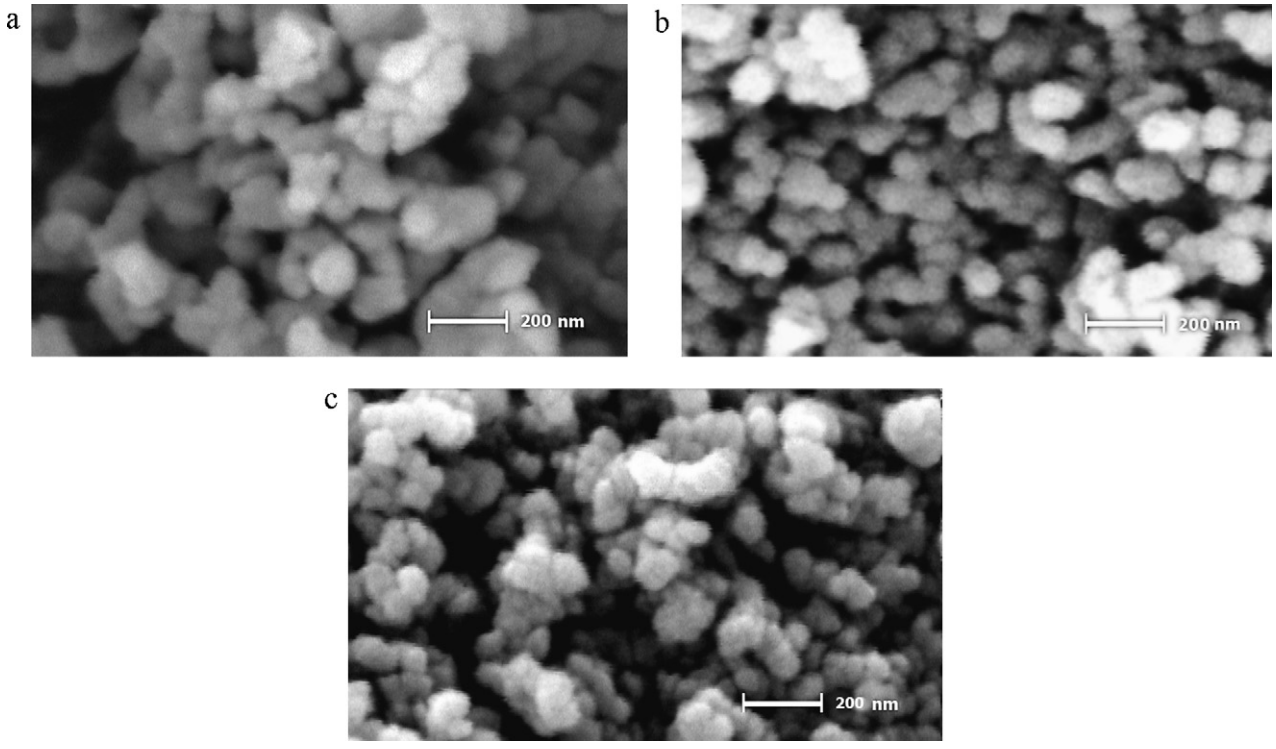

Fig. 6. SEM images of D0.0SC (a), D0.8SC (b) and D1.5SC (c).

[11,15,16,23,24,39]. This result also supports the idea that SiO_4^{4-} tetrahedra substitute PO_4^{3-} tetrahedra in the hydroxyapatite structure since CO_3^{2-} groups occupy both PO_4^{3-} and OH^- sites.

3.3. Scanning electron microscopy

Scanning electron microscopy (SEM) was used to characterize the morphology and structure of synthesized powders (discs of compact powders) before and after incubation in SBF (simulated body fluid) and cell attachment to the discs.

SEM images of the powders of both groups before incubation (Figs. 5 and 6) represent the morphology of HA and Si-HA. SEM results show a significant decrease in particle size in the Si-HA compared to pure HA (Fig. 7a and b), but there is no evidence that silicon incorporation into hydroxyapatite does affect the particle shape. Particles size obtained by image analysis (Fig. 7a and b) and crystallite size estimated by XRD data are in the same order of magnitude suggesting that

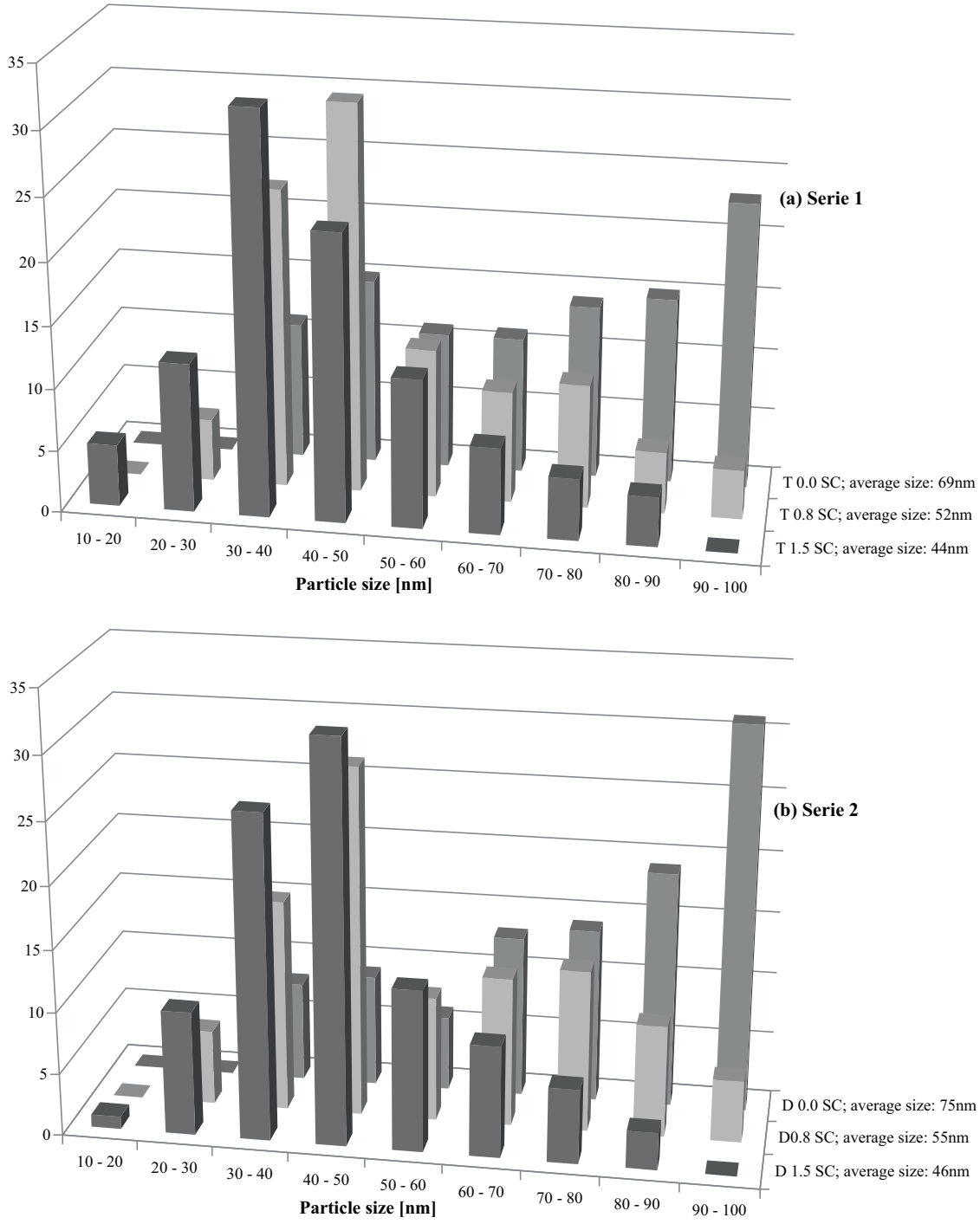

Fig. 7. Particle size distribution obtained from SEM images by NIH software, (a) series 1 and (b) series 2.

the observed particles correspond to single crystals rather than to crystal agglomerates. It should be emphasized that both methods reveal a significant particle/crystallite size reduction if 1.5 wt% SiO_2 is incorporated into the HA structure. The observed small crystal size of Si-bearing materials can be explained in terms of higher nucleation density during hydrothermal precipitation process.

3.4. In vitro assessment

As the ICP results show that Si incorporation in series 1 is more than series 2, the specimens of series 1 were chosen for in vitro tests. SEM images of the specimens of T0.0SC (pure HA) and T1.5SC (Si-HA) before and after incubation in SBF for different periods of time are shown in Fig. 8. The results show

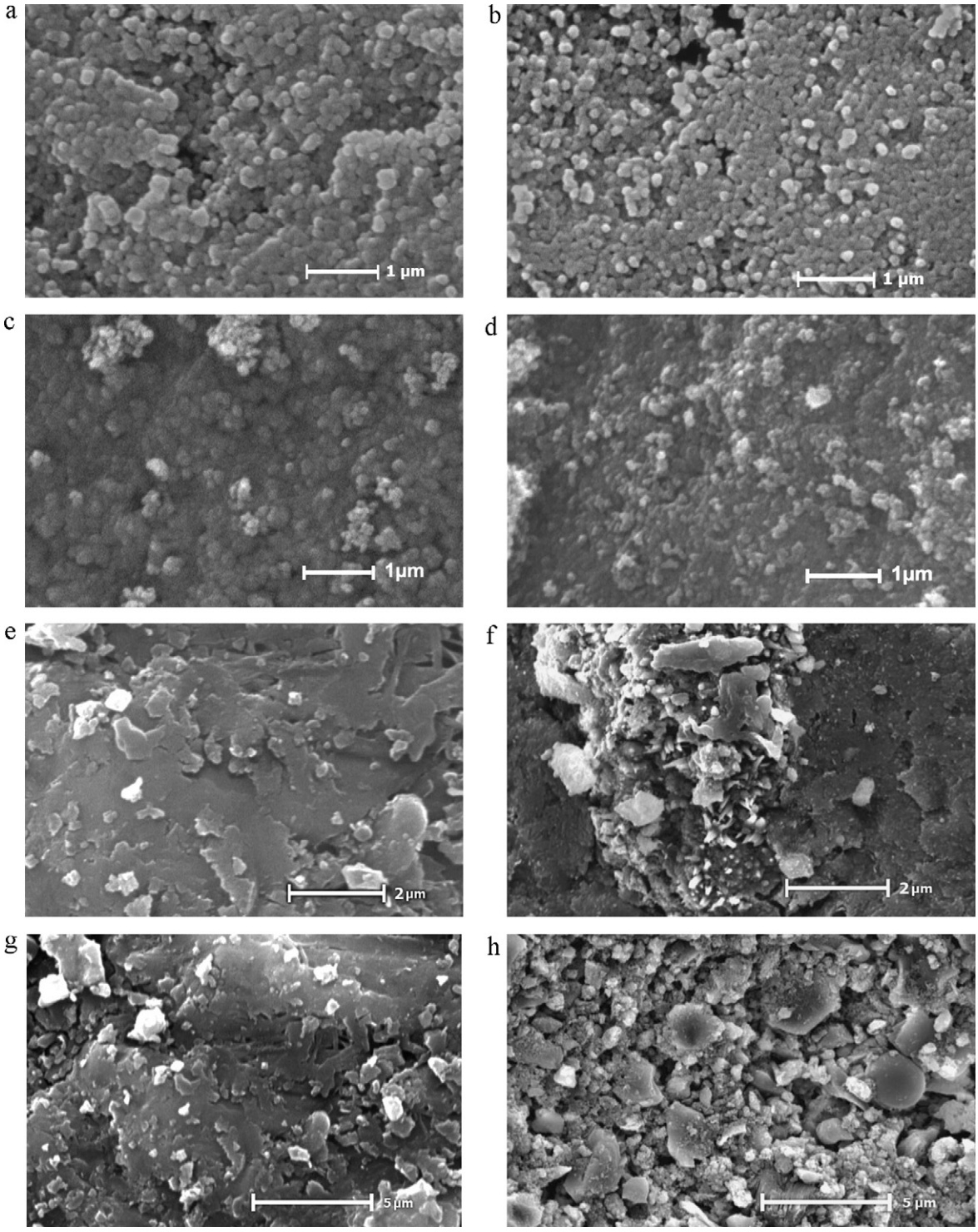

Fig. 8. SEM images of HA (T0.0SC) (a) and Si-HA (T1.5SC) (b) before incubation in SBF, HA (c) and Si-HA (d) after 3 days, HA (e) and Si-HA (f) after 8 days and HA (g) and Si-HA (h) after 14 days incubation in SBF.

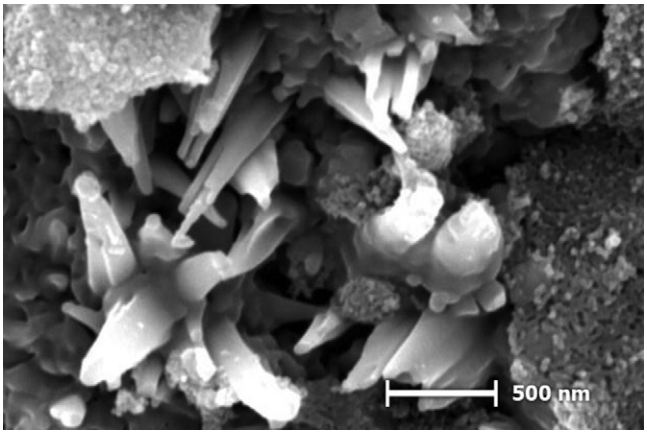

Fig. 9. SEM images of new formed HA on the surface of T1.5SC (Si-HA) sample.

nucleation of HA on the surface of specimens and the resulting morphology.

Nucleation and growth of HA is observed after 3 days in all investigated specimens, though the nucleation density is significantly higher on the surfaces of Si-HA specimens (T1.5SC). After 8 days of incubation, the Si-HA (T1.5SC) surface was partially covered by an apatite layer (Fig. 8f), while for HA (T0.0SC) significant changes were only detected after 14 days of incubation (Fig. 8g). These results may be due to a greater solubility of the Si-HA material, leading to a faster super-saturation of SBF solution and therefore a faster nucleation and growth of HA on the surface of specimen from the super-saturated SBF. These observations clearly show that biological activity of Si-HA is higher than that of reference HA. Fig. 9 shows the morphology of newly formed HA crystals (after 8 days) in higher magnification, with acicular shapes. Microstructural evidences suggest that the newly formed crystals grow with a preferential orientation.

Table 7
MTT test results on the surface of specimens and standard plastic culture surface at 570 nm after 4 days of cell culture.

Name of samples	Number of samples	Colorimetric reading Average OD (±SD)	*P* value[a]
Osteoblast on plastic surface (control)	8	0.953 (±0.029)	>0.001
Osteoblast on T0.8SC	8	0.758 (±0.020)	>0.001
Osteoblast on T1.5SC	8	0.598 (±0.035)	>0.001
Osteoblast on T0.0SC	8	0.524 (±0.026)	>0.001

[a] Independent samples test, SPSS 16.0 for windows (Release 16.0.1); each specimen was compared with human Osteoblast-like cells on plastic surfaces.

Fig. 10 shows the morphology and distribution of the attached cells on the samples (T0.0SC, T0.8SC and T1.5SC). The number of cells on the 0.8 wt% Si-HA (T0.8SC) was higher than on phase pure HA (T0.0SC) and 1.5 wt% Si-HA (T1.5SC). These observations indicate that silicon-bearing HA enhances the proliferation of human osteoblast-like cells more than silicon free HA (Fig. 10b). On the other hand it seems that

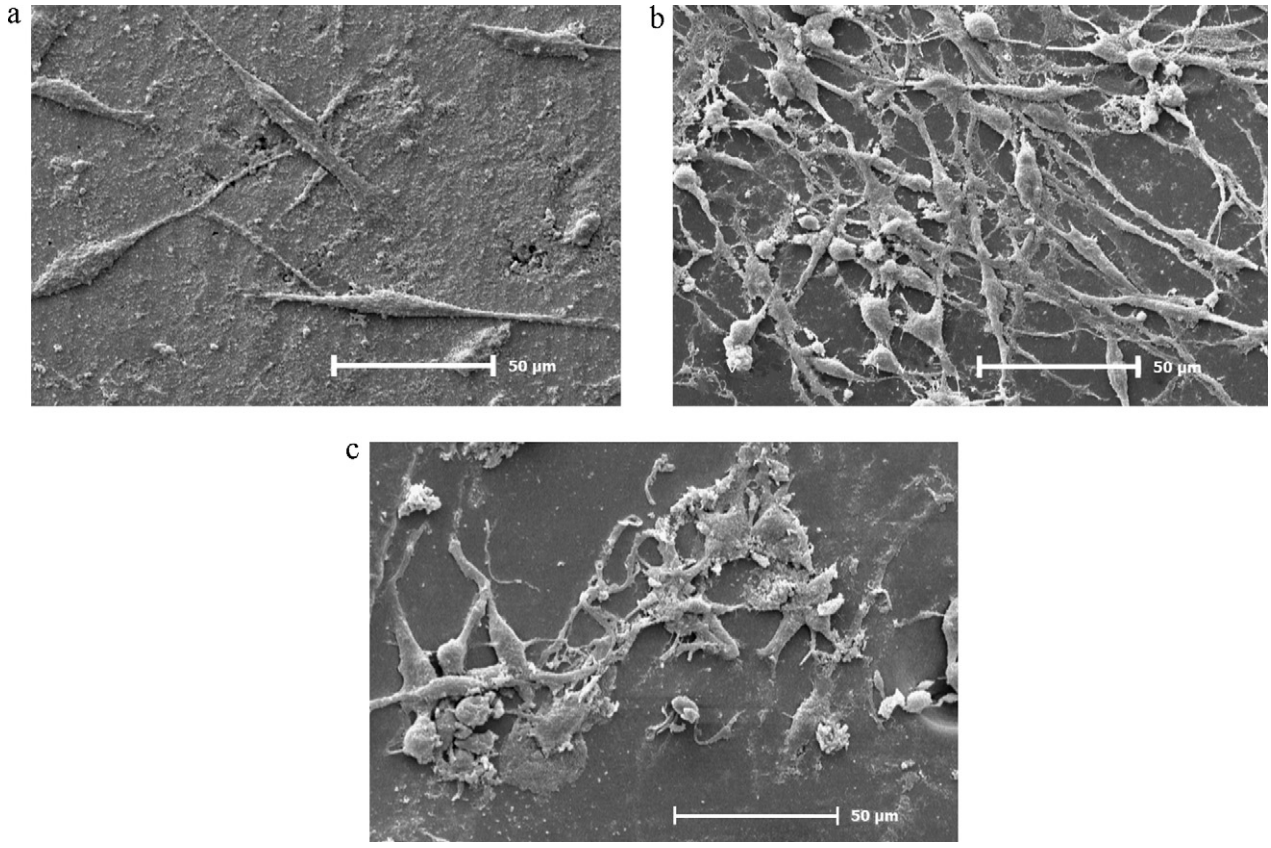

Fig. 10. SEM images of cell attachment on surface of specimens: (a) T0.0SC, (b) T0.8SC and (c) T1.5SC.

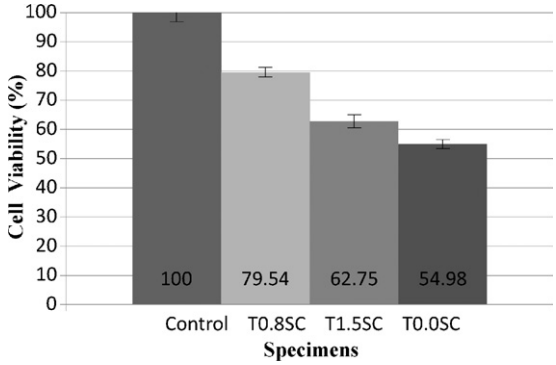

Fig. 11. Variation percentage of cells viability on the surface of specimens.

excessive amounts of incorporated Si would be counter-productive to cell attachment (Fig. 10c). The best result occurs in Si-HA of 0.8 wt% Si substitution, which may be due to the similarity with Si concentration in biological hydroxyapatite (lower than 1 wt% [7,8,11]).

MTT test results (Table 7) show that the proliferation rate of human osteoblast-like cells on the surface of 0.8 wt% Si-HA (T0.8SC) specimen is higher than that of HA samples containing 0 or 1.5 wt% SiO_2. As suggested by in vitro tests the optimum bioactivity is achieved if synthetic hydroxyapatite contains a percentage of Si that correspond to its biological counterpart. Fig. 11 shows variation percentage of cell viability on the surface of specimens and it proves that Si-HA is more bioactive than pure HA.

4. Conclusion

Approximately pure silicon-substituted hydroxyapatite powders were prosperously synthesized by the hydrothermal method using $Ca(NO_3)_2$, $(NH_4)_3PO_4$ or $(NH_4)_2HPO_4$ and $Si(OCH_2CH_3)_4$ (TEOS) as reagents. ICP analyses show the presence of Si in the structure of HA and provide evidence that the degree of Si incorporation is higher and close to expected Si content when $(NH_4)_3PO_4$ is used as the source of phosphor instead of $(NH_4)_2HPO_4$. XRD analysis of the Si-HA revealed a single, crystalline phase, similar to stoichiometric HA but with slightly different lattice constants. The presence of Si reduces the crystallinity and increases the solubility of the powder. The analysis of FTIR shows that the substitution of phosphate groups by silicate groups causes some OH^- loss to maintain the charge balance. Furthermore, SEM results show that incorporation of silicate groups reduces Si-HA particle size. The nucleation and growth of HA on Si-HA samples after incubation in SBF, occurs in shorter time as compared with pure HA samples. The results of MTT assay indicate an increase in proliferation and an increase in the number of viable human osteoblast-like cells grown on 0.8 wt% Si-HA (about 80%) compared to HA (about 55%). Based on these results, the 0.8 wt% Si-substituted hydroxyapatite has good biocompatibility and bioactivity. This composition is considered to be a useful and promising material for implants and bone substitutes.

Acknowledgements

The authors gratefully acknowledge A. Darvish, Sh. Shafiee Nezhad and J. Jafari and for their valuable help in the preparation of this manuscript.

References

[1] R.E. Unger, A. Sartoris, K. Peters, A. Motta, C. Migliaresi, M. Kunkel, U. Bulnheim, J. Rychly, C.J. Kirkpatrick, Tissue-like self-assembly in cocultures of endothelial cells and osteoblasts and the formation of microcapillary-like structures on three-dimensional porous biomaterials, J. Biomater. 28 (2007) 3965–3976.
[2] M. Salarian, M. Solati-Hashjin, S.S. Shafiei, R. Salarian, Z.A. Nemati, Template-directed hydrothermal synthesis of dandelion-like hydroxyapatite in the presence of cetyltrimethylammonium bromide and polyethylene glycol, J. Ceram. Int. 35 (2009) 2563–2569.
[3] R.J. Chung, M.F. Hsieh, R.N. Panda, T.S. Chin, Hydroxyapatite layers deposited from aqueous solutions on hydrophilic silicon substrate, J. Surf. Coatings Technol. 165 (2003) 194–200.
[4] J.H. Lee, K.S. Lee, J.S. Chang, W.S. Cho, Y. Kim, S.R. Kim, Y.T. Kim, Biocompatibility of Si-substituted hydroxyapatite, J. Key Eng. Mater. 254–256 (2004) 135–138.
[5] A.E. Porter, N. Patel, J.N. Skepper, S.M. Best, W. Bonfield, Comparison of in vivo dissolution processes in hydroxyapatite and silicon-substituted hydroxyapatite bioceramics, J. Biomater. 24 (2003) 4609–4620.
[6] S.M. Best, S. Zou, R. Brooks, J. Huang, N. Rushton, W. Bonfield, The osteogenic behaviour of silicon substituted hydroxyapatite, J. Key Eng. Mater. 361–363 (2008) 985–998.
[7] A.M. Pietak, J.W. Reid, M.J. Stott, M. Sayer, Silicon substitution in the calcium phosphate bioceramics, J. Biomater. 28 (2007) 4023–4032.
[8] E. Landi, S. Sprio, M. Sandri, A. Tampieri, L. Bertinetti, G. Martra, Development of multisubstituted apatites for bone reconstruction, J. Key Eng. Mater. 361–363 (2008) 171–174.
[9] H. Eslami, M. Solati-Hashjin, M. Tahriri, The comparison of powder characteristics and physicochemical, mechanical and biological properties between nanostructure ceramics of hydroxyapatite and fluoridated hydroxyapatite, J. Mater. Sci. Eng. C 29 (2009) 1387–1398.
[10] H. Eslami, M. Solati-Hashjin, M. Tahriri, Synthesis and characterization of nanocrystalline fluorinated hydroxyapatite powder by modified wet-chemical process, J. Ceram. Process. Res. 9 (2008) 224–229.
[11] R. Astala, L. Calderín, X. Yin, M.J. Stott, Ab initio simulation of Si-doped hydroxyapatite, J. Chem. Mater. 18 (2006) 413–422.
[12] R.Z. LeGeros, Apatite in biological systems, J. Prog. Cryst. Growth Charact. 4 (1981) 1–45.
[13] E. Landi, S. Sprio, M. Sandri, A. Tampieri, L. Bertinetti, G. Martra, Ultrastructural characterisation of hydroxyapatite and silicon-substituted hydroxyapatite, J. Key Eng. Mater. 361–363 (2008) 171–174.
[14] E.S. Thian, J. Huang, S.M. Best, Z.H. Barber, W. Bonfield, Surface wettability enhances osteoblast adhesion on silicon-substituted hydroxyapatite thin films, J. Key Eng. Mater. 330–332 (2007) 877–880.
[15] C.M. Botelho, M.A. Lopes, I.R. Gibson, S.M. Best, J.D. Santos, Structural analysis of Si-substituted hydroxyapatite: zeta potential and X-ray photoelectron spectroscopy, J. Mater. Sci.: Mater. Med. 13 (2002) 1123–1127.
[16] X.L. Tang, X.F. Xiao, R.F. Liu, Structural characterization of silicon-substituted hydroxyapatite synthesized by a hydrothermal method, J. Mater. Lett. 59 (2005) 3841–3846.
[17] A. Aminian, Effect of silicon substitution on bioactivity of hydrothermal synthesized of hydroxyapatite nano-powders, M.Sc. Thesis, Amirkabir University of Technology, Tehran, Iran, 2009.
[18] T. Tian, D. Jiang, J. Zhang, Q. Lin, Synthesis of Si-substituted hydroxyapatite by a wet mechanichemical method, J. Mater. Sci. Eng. C 28 (2008) 57–63.
[19] S.V. Dorozhkin, E.I. Dorozhkina, F.N. Oktar, S. Salman, A simplified preparation method of silicon-substituted calcium phosphates according to green chemistry principles, J. Key Eng. Mater. 330–332 (2007) 55–58.

[20] M. Aizawa, N. Patel, A.E. Porter, S.M. Best, W. Bonfield, Syntheses of silicon-containing apatite fibres by a homogeneous precipitation method and their characterization, J. Key Eng. Mater. 309–311 (2006) 1129–1132.
[21] P.A.A.P. Marques, M.C.F. Magalhaes, R.N. Correia, M. Vallet-Regi, Synthesis and characterization of silicon-substituted hydroxyapatite, J. Key Eng. Mater. 192–195 (2001) 247–250.
[22] N. Patel, E.L. Follon, I.R. Gibson, S.M. Best, W. Bonfield, Comparison of sintering and mechanical properties of hydroxyapatite and silicon-substituted hydroxyapatite, J. Key Eng. Mater. 240–242 (2003) 919–922.
[23] C.M. Botelho, R.A. Brooks, T. Kawai, S. Ogata, C. Ohtsuki, S.M. Best, M.A. Lopes, J.D. Santos, N. Rushton, W. Bonfield, In vitro analysis of protein adhesion to phase pure hydroxyapatite and silicon substituted hydroxyapatite, J. Key Eng. Mater. 284–286 (2005) 461–464.
[24] E.L. Solla, F. Malz, P. González, J. Serra, C. Jaeger, B. León, The role of Si substitution into hydroxyapatite coatings, J. Key Eng. Mater. 361–363 (2008) 175–178.
[25] S.R. Kim, J.H. Lee, Y.T. Kim, D.H. Riu, S.J. Jung, Y.J. Lee, S.C. Chung, Y.H. Kim, Synthesis of Si,Mg substituted hydroxyapatites and their sintering behaviors, J. Biomater. 24 (2003) 1389–1398.
[26] I.R. Gibson, K.A. Hing, S.M. Best, W. Bonfield, Enhanced in vitro cell activity and surface apatite layer formation on novel silicon substituted hydroxyapatites, in: H. Ohgushi, G.W. Hastings, T. Yoshikawa (Eds.), Proceeding of the 12th International Symposium on Ceramics in Medicine, Nara, Japan, (1999), pp. 191–194.
[27] J.W. Reid, L. Tuck, M. Sayer, K. Fargo, J.A. Hendry, Synthesis and characterization of single-phase silicon-substituted α-tricalcium phosphate, J. Biomater. 27 (2006) 2916–2925.
[28] M. Saki, M.K. Narbat, A. Samadikuchaksaraei, H.B. Ghafouri, F. Gorjipour, Biocompatibility study of a hydroxyapatite-alumina and silicon carbide composite scaffold for bone tissue engineering, J. Yakhteh 11 (1) (2009) 55–60.
[29] J.A. Stephen, J.M.S. Skakle, I.R. Gibson, Synthesis of novel high silicate-substituted hydroxyapatite by Co-substitution mechanisms, J. Key Eng. Mater. 330–332 (2007) 87–90.
[30] L.L. Hench, Sol–Gel Silica Properties, Processing and Technology Transfer, Chapter 10, Biological Implications, 1999, pp. 116–163.
[31] C.M. Botelho, R.A. Brooks, S.M. Best, M.A. Lopes, J.D. Santos, N. Rushton, W. Bonfield, Biological and physical–chemical characterization of phase pure HA and Si-substituted hydroxyapatite by different microscopy techniques, J. Key Eng. Mater. 254–256 (2004) 845–848.
[32] A.J. Ruys, Silicon-doped hydroxyapatite, J. Aust. Ceram. Soc. 29 (1993) 71–80.
[33] L. Boyer, J. Carpena, J.L. Lacou, Synthesis of phosphate-silicate apatites at atmospheric pressure, J. Solid State Ionics 95 (1997) 121–129.
[34] I.R. Gibson, S.M. Best, W. Bonfield, Chemical characterization of silicon-substituted hydroxyapatite, J. Biomed. Mater. Res. 4 (1999) 422–428.
[35] M.C. Andradea, M.R. Tavares Filgueirasa, T. Ogasawarab, Hydrothermal nucleation of hydroxyapatite on titanium surface, J. Eur. Ceram. Soc. 22 (2002) 505–510.
[36] M. Palard, E. Champion, S. Foucaud, Synthesis of silicate hydroxyapatite $Ca_{10}(PO_4)_{6-x}(SiO_4)_x(OH)_{2-x}$, J. Solid State Chem. 181 (2008) 1950–1960.
[37] R. Ravarian, F. Moztarzade, M. Solati Hashjin, S.M. Rabiee, P. Khoshakhlagh, M. Tahriri, Synthesis, characterization and bioactivity investigation of bioglass/hydroxyapatite composite, J. Ceram. Int. 36 (2009) 291–297.
[38] T. Kokubo, Apatite formation on surfaces of ceramics, metals and polymers in body environment, J. Acta Mater. 46 (1998) 2519–2527.
[39] E. Landi, A. Tampieri, G. Celotti, S. Sprio, Densification behavior and mechanisms of synthetic hydroxyapatite, J. Eur. Ceram. Soc. 20 (2000) 2377–2387.
[40] D. Arcos, J. Rodríguez-Carvajal, M. Vallet-Regí, The effect of the silicon incorporation on the hydroxylapatite structure. A neutron diffraction study, J. Solid State Sci. 6 (2004) 987–994.
[41] K.A. Hing, P.A. Revell, N. Smith, T. Buckland, Effect of silicon level on rate, quality and progression of bone healin within silicate-substituted porous hydroxyapatite scaffolds, J. Biomater. 27 (2006) 5014–5026.
[42] H.B. Shi, H. Zhong, Y. Liu, F.Z. Zhang, M.C. Liang, M. Chen, Preparation of silicate substituted calcium deficient hydroxyapatite by coprecipitation, J. Key Eng. Mater. 330–332 (2007) 83–86.